ELSEVIER

Marine Geology 248 (2008) 193–212

MARINE GEOLOGY
INTERNATIONAL JOURNAL OF MARINE GEOLOGY, GEOCHEMISTRY AND GEOPHYSICS

www.elsevier.com/locate/margeo

Sandwave migration in Monterey Submarine Canyon, Central California

J.P. Xu [a,*], Florence L. Wong [b], Rikk Kvitek [c], Douglas P. Smith [c], Charles K. Paull [d]

[a] U.S. Geological Survey, Pacific Science Center, Santa Cruz, CA 95060 USA
[b] U.S. Geological Survey, Coastal and Marine Geology, Menlo Park, CA 94025 USA
[c] California State University Monterey Bay, Seaside, CA 93955 USA
[d] Monterey Bay Aquarium Research Institute, Moss Landing, CA 95039 USA

Received 1 June 2007; received in revised form 5 November 2007; accepted 8 November 2007

Abstract

Repeated high-resolution multibeam bathymetric surveys from 2002 through 2006 at the head of the Monterey Submarine Canyon reveal a sandwave field along the canyon axis between 20 and 250 m water depth. These sandwaves range in wavelength from 20 to 70 m and 1 to 3 m in height. A quantitative measure was devised to determine the direction of sandwave migration based on the asymmetry of their profiles. Despite appreciable spatial variation the sandwaves were found to migrate in a predominantly down-canyon direction, regardless of season and tidal phases. A yearlong ADCP measurement at 250 m water depth showed that intermittent internal tidal oscillations dominated the high-speed canyon currents (50–80 cm/s), which are not correlated with the spring–neap tidal cycle. Observed currents of 50 cm/s or higher were predominantly down-canyon. Applying a simple empirical model, flows of such magnitudes were shown to be able to generate sandwaves of a size similar to the observed ones.

Keywords: submarine canyons; sandwaves; migration

1. Introduction

Monterey Canyon is the largest submarine canyon off the west coast of the United States. An annual volume of $200–500 \times 10^3$ m^3 of sediment estimated from longshore drift and river discharge (Best and Griggs, 1991; Eittreim et al., 2002) is assumed to enter the head of the canyon. Various transport mechanisms of such sediment, including turbidity or sediment flows (Normark and Piper, 1991; Garfield et al., 1994; Okey, 1997; Xu et al., 2004) and mass wasting or submarine landslides (Greene and Ward, 2003) have been observed or proposed for Monterey Canyon, but there is still no established link between the sediment accumulation at the canyon head and the vast Monterey fan and valley complex (Normark and Carlson, 2003; Fildani and Normark, 2004). Sandwaves (or dunes) are a major sediment transport mechanism in many subaerial (eolian) and subaqueous (marine or fluvial) environments (Allen, 1982). They develop as a result of an inherent instability of sand beds forced by water flows (Besio et al., 2004); thus the size, shape, and other properties of the sandwaves depend on the driving force, water depth, and sediment grain size (Rubin and

* Corresponding author.
E-mail address: jpx@usgs.gov (J.P. Xu).

0025-3227/$ - see front matter © 2007 Elsevier B.V. All rights reserved.
doi:10.1016/j.margeo.2007.11.005

McCulloch, 1980; Ashley, 1990; Francken et al., 2004; Bartholdy et al., 2005). Not until recently did surveys with advanced sounding and navigational technology reveal the existence of a field of large sandwaves along the axis of the Monterey Submarine Canyon (Smith et al., 2005, 2007). Such high-resolution, centimeter-scale swath-bathymetry enables researchers to not only study the spatial variation, but also, if repeated frequently enough, examine the temporal changes of the sandwave fields (Knaapen, 2005; Wienberg and Hebbeln, 2005; Ernstsen et al., 2005; Barnard et al., 2006; Ernstsen et al., 2006; Smith et al., 2007). Furthermore, the bathymetric data provides researchers with the opportunity to characterize the lateral (across-channel) variations of the sandwaves (Ernstsen et al., 2005).

Sandwave migration is both a major component of bedload sediment transport (Dalrymple, 1984; Van den Berg, 1987; Hoekstra et al., 2004) and of a great concern to navigation and coastal infrastructure safety (Katoh et al., 1998; Morelissen et al., 2003), but is also very difficult to quantify. Existing models of sandwave migration (Nemeth et al., 2002; Besio et al., 2004) appear to work well only in certain cases (Knaapen, 2005). To the present studies of sandwave migration are mostly site-specific and observation-based. In this paper, we analyze a sequence of high-resolution swath-bathymetry surveys of sandwaves in the axis of the Monterey Submarine Canyon collected over a 5-year period (2002–2006). We devise a method to quantify the direction of the sandwave migration. By characterizing the morphology and dynamics of sandwaves and their temporal changes and spatial patterns, we attempt to establish a relationship between the canyon hydrodynamics, sandwave migrations, and sediment transport along the canyon axis. The majority of the bedforms here fall into the category of "large dunes" (Ashley, 1990). However we choose to use the term "sandwave" throughout the paper because (1) it better conforms with the more restricted meanings of tidal bedforms associated with reversing sediment transport (Allen, 1980), and (2) it was used in previous publications of the same data set (Smith et al., 2005, 2007).

2. Data and methods

2.1. Bathymetric surveys

From 2002 to 2006, the Seafloor Mapping Laboratory of the California State University Monterey Bay (CSUMB) conducted a series of bathymetric surveys at the head of the Monterey Submarine Canyon between water depths 20 and 300 m (Table 1). Although two different boats were used in the seven surveys listed, the setup of the multibeam system, a Reson 8101 244 kHz multibeam sonar instrument, was the same (see Smith et al., 2005, for technical details). High-resolution dual frequency differential GPS systems (Trimble 4700, Trimble 5700 or cNav Navcom 2050) were used in all surveys to achieve submeter horizontal positioning precision. Except for the first survey in 2002, these same GPS systems were used to provide high-resolution vertical corrections for tidal variation during the surveys so the measured vertical precision reached 0.2 m or better. After rigorous manual editing to remove spurious data points, the data were gridded into 3-m interval XYZ format from which both shaded relief images (Fig. 1) and digital elevation models (DEMs) were produced. The bathymetric profiles of the sandwave field along the several lines parallel to the canyon floor (Fig. 2) were obtained from ArcInfo, a software package that processes spatial information of the DEMs. The ensuing discussion of sandwave migration is based on these 3-m resolution bathymetric data sets.

Table 1
The seven multibeam surveys conducted by CSUMB

Survey no.	Date	Tide phase
1	03/26–27/2003	Spring
2	09/13/2003	Neap
3	09/17/2004	Neap
4	11/19/2004	2 days before neap
5	02/04–05/2005	3 days before spring
6	09/09/2005	3 days after neap
7	02/23/2006	5 days after neap

Each survey spanned at least one working day. The tidal phase during each survey was obtained from the Monterey Harbor gage (http://tidesandcurrents.noaa.gov). The collected data typically have resolution of 3 m in horizontal and 0.2 m in vertical.

2.2. Oceanographic mooring observations

A subsurface mooring was deployed at 245 m water depth in the axis of the upper Monterey Canyon, near the down-canyon boundary of the multibeam survey (Fig. 1). The mooring contained a downward-looking acoustic Doppler current profiler (ADCP) at ~70 m above bed (MAB) and two instrument packages (temperature, salinity, transmissometer, and sediment trap) at 30 MAB and 80 MAB respectively (Table 2). The purpose of the mooring was to collect in-situ measurements of sediment transport events by turbidity currents (Xu et al., 2004) and tidal and/or internal tidal currents that are related to the formation and migration of the sandwaves revealed in the multibeam surveys. The downward-looking ADCP recorded one ensemble (an average of 60 1-s pings) every 10 min at 33 bins (elevations) that are 2 m apart.

Due to the strong reflections from the canyon floor or sometimes the walls the velocity data from the lowest three bins (bin 31 to 33) are very noisy. Bin 30 at ~4 m above the canyon floor and all other shallower bins have velocity data of good quality. The sampling frequency of the temperature/salinity sensors varied depending on their power usage but they all had sampling intervals shorter than 10 min. The mooring was deployed on May 16, 2005, and recovered on July 5, 2006. Except for the ADCP that ran out of battery power in mid-June 2006, all other instruments recorded useable data for the 14-month deployment.

2.3. Quantifying the direction of sandwave migration

In general, sandwaves migrate in the direction of the maximum sand transport. In fluvial (Coleman, 1969) and ebb- or flood-dominated inlet (Ernstsen et al., 2005) channels, the direction of sandwave migration is known and the speed of the migration may be modeled (Allen, 1968; Knaapen, 2005) or measured (Ernstsen et al., 2005). On the sea floor near the head of the Monterey Canyon where semi-diurnal tidal flow dominates and has no apparent asymmetry, determining the direction of sandwave migration is more difficult. Comparing sequential multibeam images to determine migration direction seems to work in a small area but fails in the surrounding areas (Smith et al., 2007). Depending on the time interval between multibeam surveys, there may also be an "aliasing" (not strictly the definition of aliasing here, rather an error resulting from a sandwave having moved more than a full wavelength during two surveys) effect with this method.

Here we attempt to introduce a quantitative way to determine sandwave migration direction. This method assumes that the migration direction is correlated to the asymmetry of the sandwaves (Fig. 3). For asymmetrical sandwaves (Fig. 3-A) the first derivative (gradient), $d\eta/dx$, of the sandwave profiles can be calculated, which displays a non-linear wave form (Fig. 3-B). After calculating the amplitude h (with signs) and the zero-crossing length L of the $d\eta/dx$ wave form in Fig. 3-B, a pair of values of the h/L ratio (with signs) are obtained for each individual sandwave (Fig. 3-C). The "asymmetry index" is defined

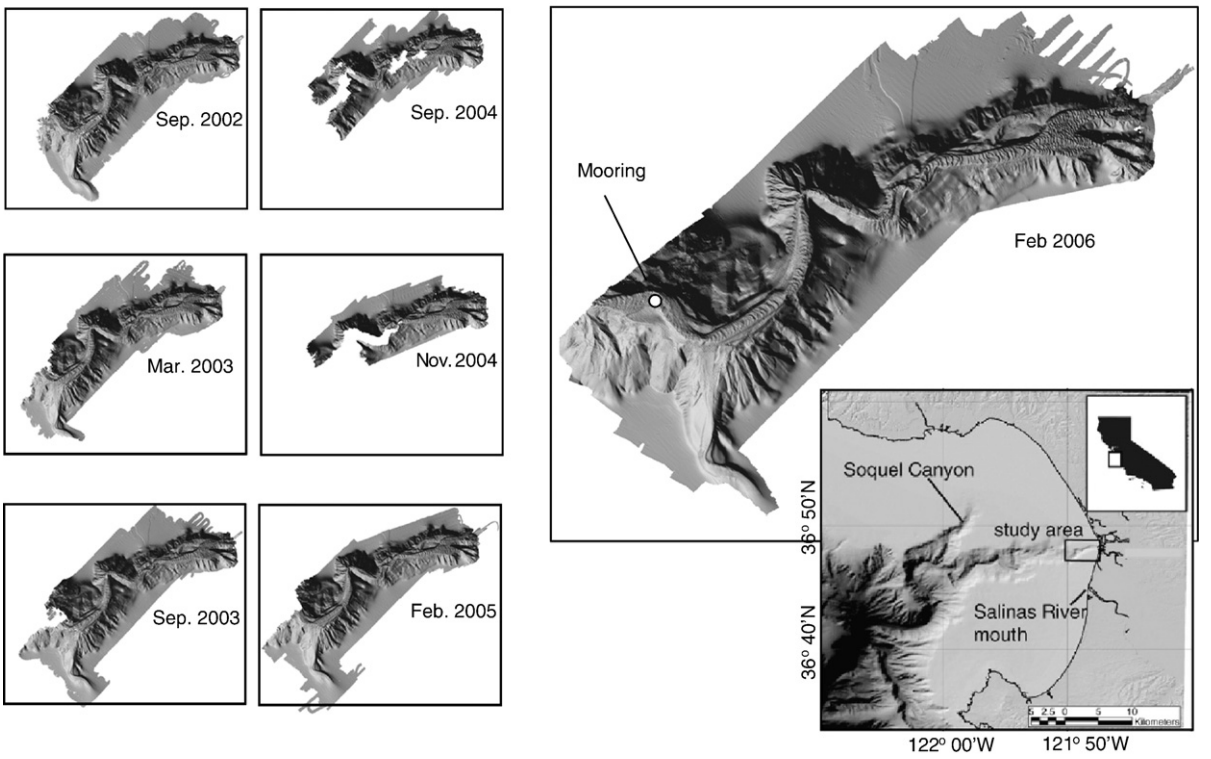

Fig. 1. Seven shaded relief images of the multibeam bathymetric data collected from 2002 through 2006 at the head of the Monterey Submarine Canyon off central California. The image from the most recent survey (February 2006) is enlarged to show details of the sandwaves and the site of the mooring deployed from 2005 to 2006.

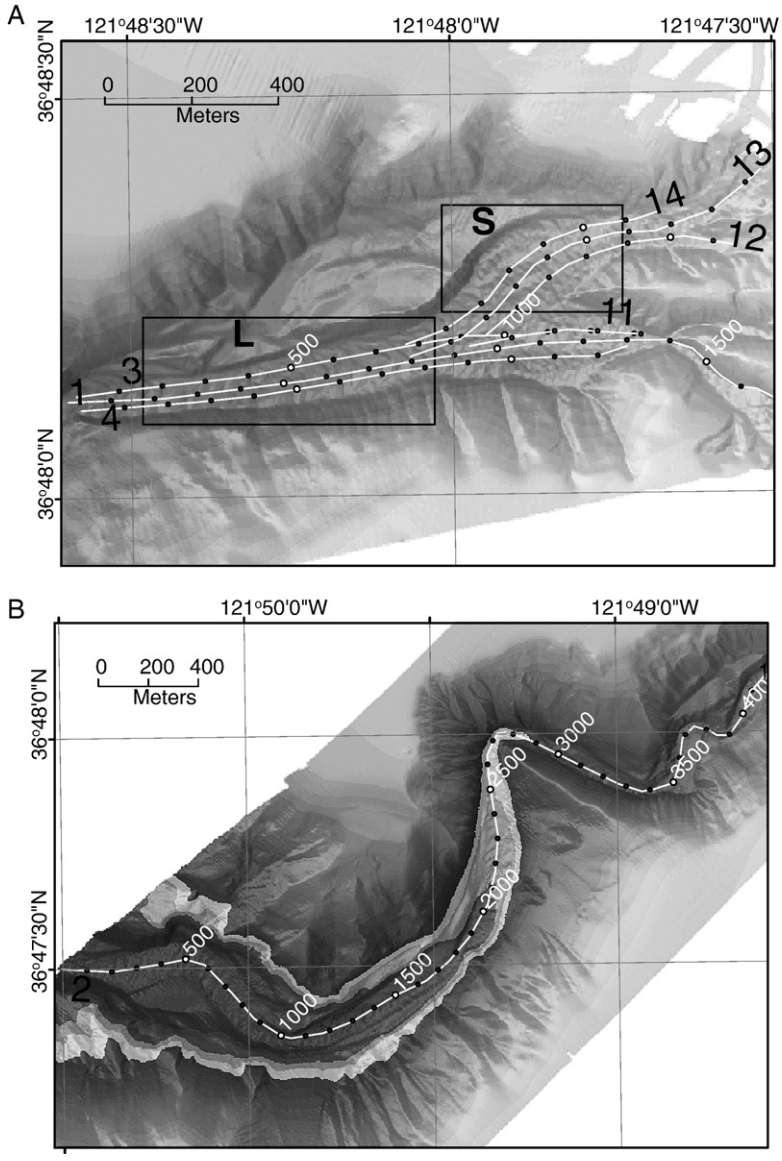

Fig. 2. Lines of profiles overlaid on the February 2006 multibeam shaded relief image. (A) Three lines lie in the main channel and two lie in upper canyon tributaries (one along the axis, one each near the toe of the canyon wall on either side). (B) Only the axial line is used in the deeper part of the canyon (280–150 m). Black letters denote the line numbers, and white letters are distance in meters from the beginning of each line. Solid dots mark the 100 m distance interval, and the empty circles mark the 500 m distance interval. The two rectangles in the upper panel are areas of large (L) and small (S) sandwaves.

as the sum of the h/L pairs for each sandwave. A positive asymmetry index means that the sandwave migrates to the left, and a negative index represents migration to the right. In the case of the Monterey canyon, a positive index means sandwaves are migrating down-canyon and vice versa.

This method is applied to the seven multibeam images of the head of the Monterey submarine canyon to assess the general direction of the sandwave migration. Track lines are drawn along the canyon's main channel and tributaries (Fig. 2) to obtain the sandwave profiles from the multibeam bathymetric data. Sandwave profiles from seven track lines are analyzed. The slope of the canyon floor is removed from the bathymetric data before the first derivative is calculated. Removing the slope alters the values of the first derivative, but if the sign of the asymmetry index is positive (downslope migration) after removing the bed slope, the sign of the asymmetry index would also have been positive without removing the bed slope (Fig. 4-A). On the other hand, when the sign of the asymmetry index is negative (upslope migration) after

Table 2
Configurations of the instruments on the Monterey Canyon mooring, deployed on May 13, 2005, at 245 m water depth

Instrument	Measurement	Height (MAB)	Configuration
ADCP	Currents, temperature	70	Sampling interval: 10 min. ADCP bin size: 2 m
Seacat/Microcat	Temperature, salinity	30, 80	Sampling interval: 10 min.
Transmissometer	turbidity	30, 80	Sampling interval: 10 min.
Sediment trap	Sediment sample	30, 80	

Lat: 36 47.452'N, Lon: 121 50.189'W. The mooring was recovered on July 5, 2006.

removing the bed slope, results may conflict with calculations for original topography (Fig. 4-B).

3. Results

3.1. Bottom flows near the head of the Monterey Canyon

Currents with tidal frequencies are the main driving forces in submarine canyons. This includes both the barotropic and baroclinic tidal currents. Due to the great depths and complex topography in submarine canyons, technological and logistic difficulties have precluded oceanographic measurements that would have been easily obtained in other environments such as continental shelves. Several such measurements do exist in the Monterey Canyon (Petruncio et al., 1998; Key, 1999; Xu et al., 2002; Paull et al., 2003), but they were mainly in much deeper water. Except for two other ADCP measurements (Key, 1999) the mooring data presented here are the only bottom flow measurements at the head of the Monterey Canyon near the multibeam survey area.

Monterey Bay experiences a mixed tide that contains four major astronomical tidal constituents: two in the diurnal group (O1, K1) and two in the semi-diurnal group (M2, S2). Tidal analysis shows that the total amplitude of the semi-diurnal tide is in general higher than the amplitude of the diurnal tide in Monterey Bay. Due to the slight frequency difference between two constituents in each group (diurnal or semi-diurnal), the beating of the two constituents in each group creates the fortnightly spring–neap cycle. In addition, the beating between the two groups produces a much longer cycle in which the biggest spring-tidal range and the smallest neap-tidal range co-

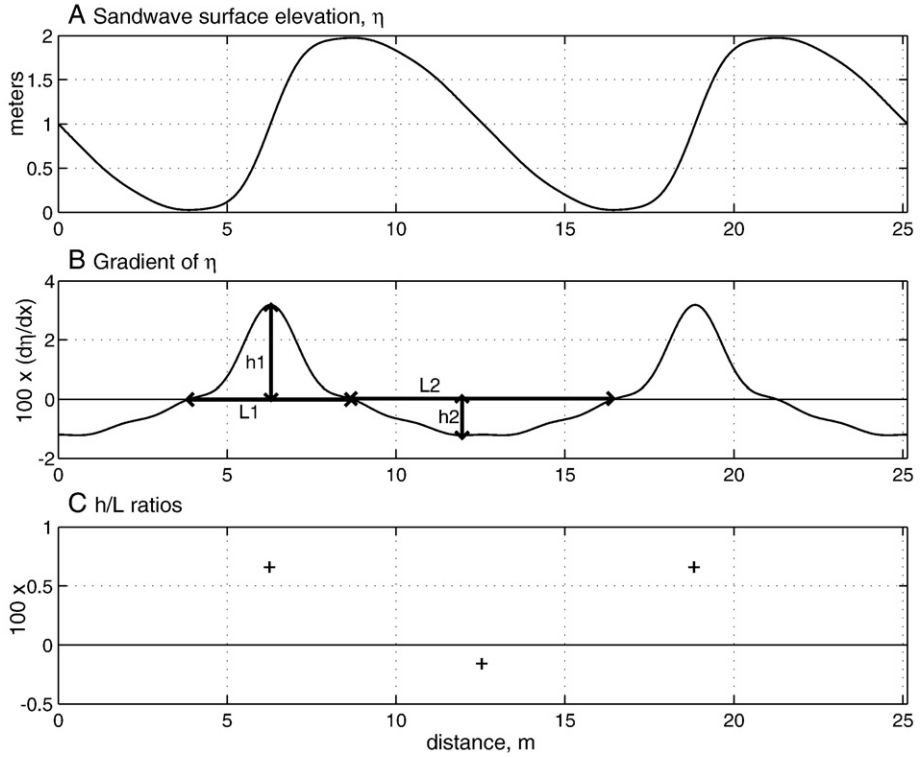

Fig. 3. Correlation of sandwave migration direction with wave asymmetry. (A) a train of asymmetrical sandwaves generated with a formula modified from Drake and Calantoni (2001), $\eta = \sin\left(\frac{x}{2}\right) + 0.75\sum_{n=2}^{6} \frac{1}{2^n} \sin\left(\frac{2x}{n} - (n-1)\pi\right)$, where x=(0:0.01:20)π. (B) the first derivative (gradient) of η. (C) the ratio of h/L (height/wavelength). The asymmetry index is the sum of the h/L pair for each individual sandwave.

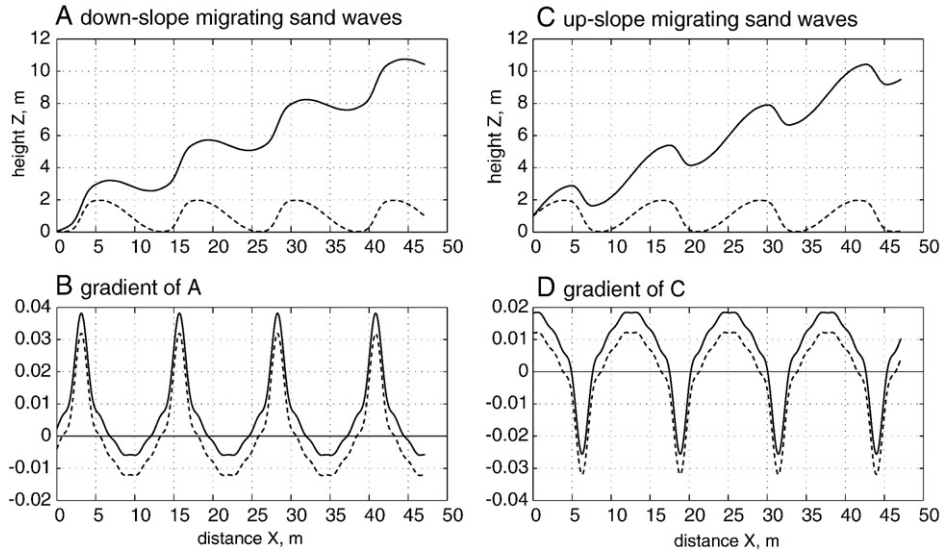

Fig. 4. (A, C) Vertical profiles of migrating sandwaves with and without a slope and (B, D) the effect of the slope on the sandwave asymmetry index. The existence of a slope enhances the asymmetry of downslope migrating sandwaves, but reduces the asymmetry of upslope migrating sandwaves.

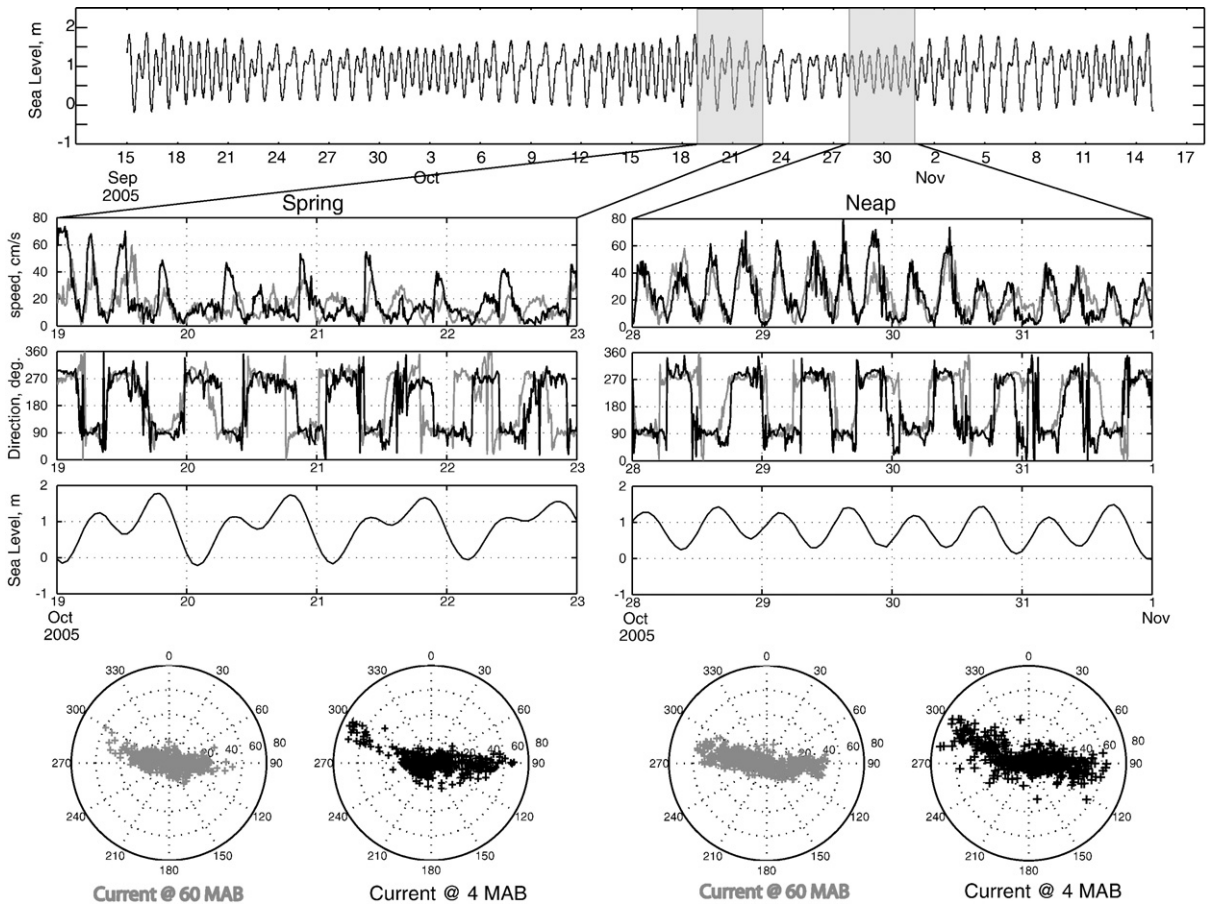

Fig. 5. Composite plots of measured sea level at the Monterey Harbor gauge and measured currents from the ADCP mooring site during a spring and neap tide in October 2005 when the spring tide is the weakest and the neap tide is the strongest. The bottom panels are scatter plots of the same data showing both the magnitude and direction of the measured currents at 4 and 60 MAB, respectively.

exist in January and July, and the smallest spring-tidal range and the biggest neap-tidal range coexist in April and October. Figs. 5 and 6 show the tide gauge measurement in Monterey Harbor (http://tidesonline.nos.noaa.gov) and associated currents measured from the USGS mooring in the canyon. In October 2005 when the spring–neap difference is the weakest, the tidal range was less than 2.0 m during spring tides and slightly greater than 1.0 m during neap tides. In January 2006, the tidal range reached 2.5 m during spring tide but was only 1.0 m during the neap.

The strength of the tidal currents measured at the mooring site was not directly proportional to the tidal range that is represented by the Monterey Harbor gauge. Although the current speed within the canyon was almost twice as high during spring tide as during neap in January 2006 (Fig. 6), the neap-tidal current during October 2005 was actually stronger, especially higher in the water column, than the spring-tidal current (Fig. 5). This indicates that besides the barotropic tides other processes such as internal tides contribute significantly in generating the measured tidal currents in the canyon. The internal tides are probably also responsible for the intensification of the currents towards the canyon floor. This bottom intensification is always present, but the magnitude varies from time to time without apparent relation to the spring–neap cycle (e.g., strong intensification during spring tide in October 2005 and during neap tide in January 2006). However, the strongest bottom intensification occurs primarily when the canyon currents flow up-canyon reflecting the combined effects of canyon topography and the up-canyon energy transfer by internal tides (Petruncio et al., 1998).

The measured currents were asymmetric in both direction and speed (scatter polar plots in Figs. 5 and 6). The up-canyon currents were in general directed to 90°T (i.e., East), but the down-canyon currents were directed between 270°T and 300°T depending on the speed. The stronger the current speed, the closer to 300°T the current direction. The directional asymmetry appears to be caused mainly by the steering effects of the canyon walls. The mooring was

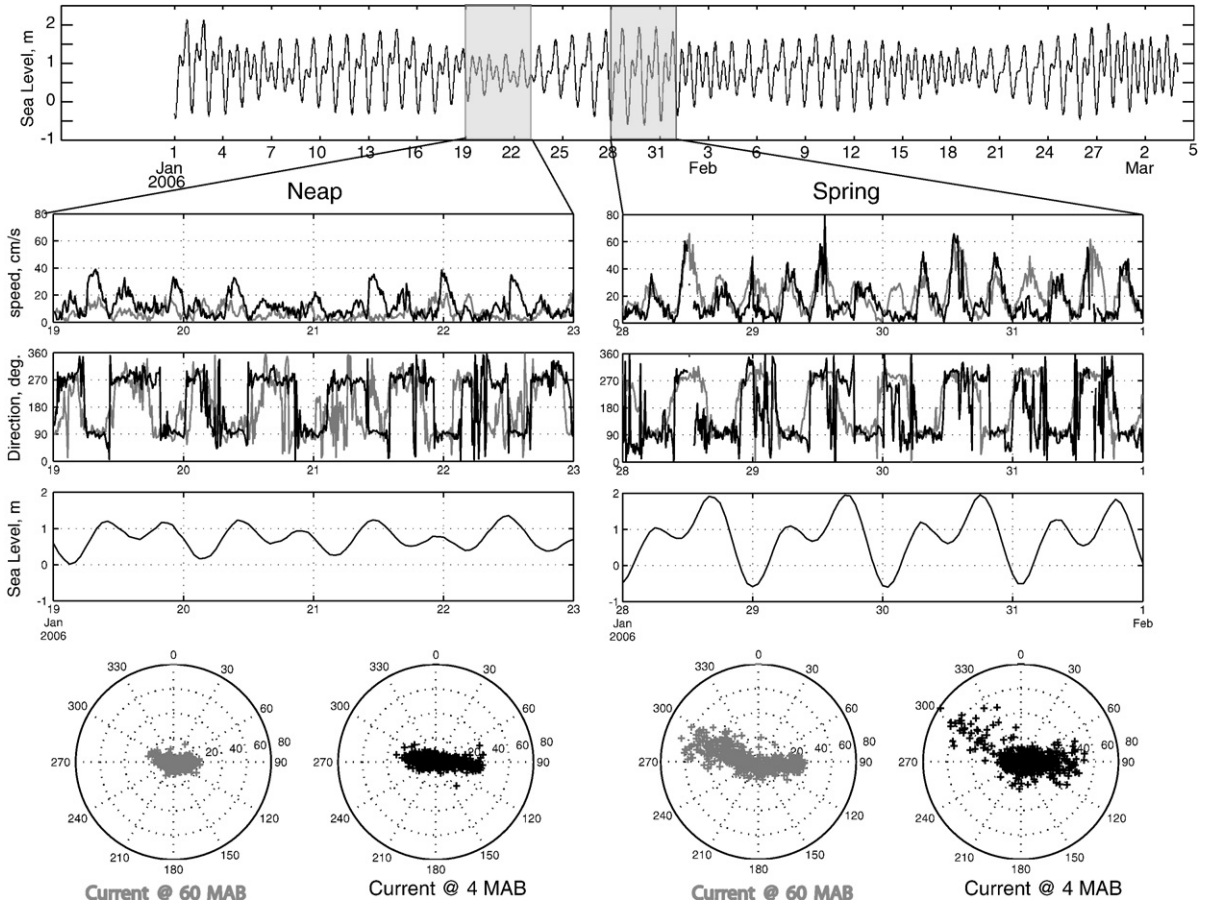

Fig. 6. Plots of measured sea level as explained in Fig. 5, but for spring and neap tides in January 2006 when the spring tide is deemed to be the strongest and the neap tide is the weakest.

deployed at a relatively wide and flat area that happens to be close to a turn of the canyon axis. Both the up-and down-canyon currents need to negotiate the turn near the mooring site. The faster the current speed, the more difficult it is to make the turn, thus momentum of currents with higher speed maintained the direction of the canyon section before the turn, a centrifugal acceleration process well known in river meanders and curved channels (Leopold and Wolman, 1960; Kalkwijk and Booij, 1986). Similar asymmetry was also found in other places of the canyon (Key, 1999). The four 4-day measured currents examined in Figs. 5 and 6 generally represent the end members (highest spring and lowest neap) of the tidal current variation at the mooring site. Although not always the case, the down-canyon currents had higher speeds than the up-canyon currents, especially higher in the water column (60 MAB). For the near-bed currents (4 MAB), the 60-cm/s or higher speed was more down-canyon than up-canyon. This is further illustrated by the histograms of the along-canyon currents measured 4 MAB (Fig. 7). Since the "along-canyon" orientations are different for down-and up-canyon flows, the flow asymmetry is established by comparing the rotated down-canyon flows against the non-rotated east currents. During the 1-year deployment, the maximum speed of the measured tidal current at the mooring site was 80 cm/s.

Internal tides are a dominant driving force within the Monterey submarine canyon (Petruncio et al., 1998; Key, 1999; Kunze et al., 2002). The observed tidal currents at the mooring site are mostly due to the propagating internal tides that are at least an order of magnitude more energetic in the canyon than their barotropic counterparts (Petruncio et al., 1998). Two typical time-series of measured currents due to internal tides are plotted in Fig. 8. The first type is similar to the flow patterns that are caused by non-linear internal bores (Key, 1999). The internal bores occur as packets that may span several days, but the timing of these internal bore packets has no apparent relationship with the spring–neap cycle. In each of these packets strong up-canyon acceleration, coinciding with sudden temperature drops, occurs with a semi-diurnal frequency (Fig. 8). The sudden drop of temperature by 0.8 degrees takes place within about 20 min while the up-canyon flow reaches the highest speed of 50–60 cm/s. It then takes the rest of the half semi-diurnal cycle (6 h) for the current to reach slack while the temperature continues to decrease another 0.8

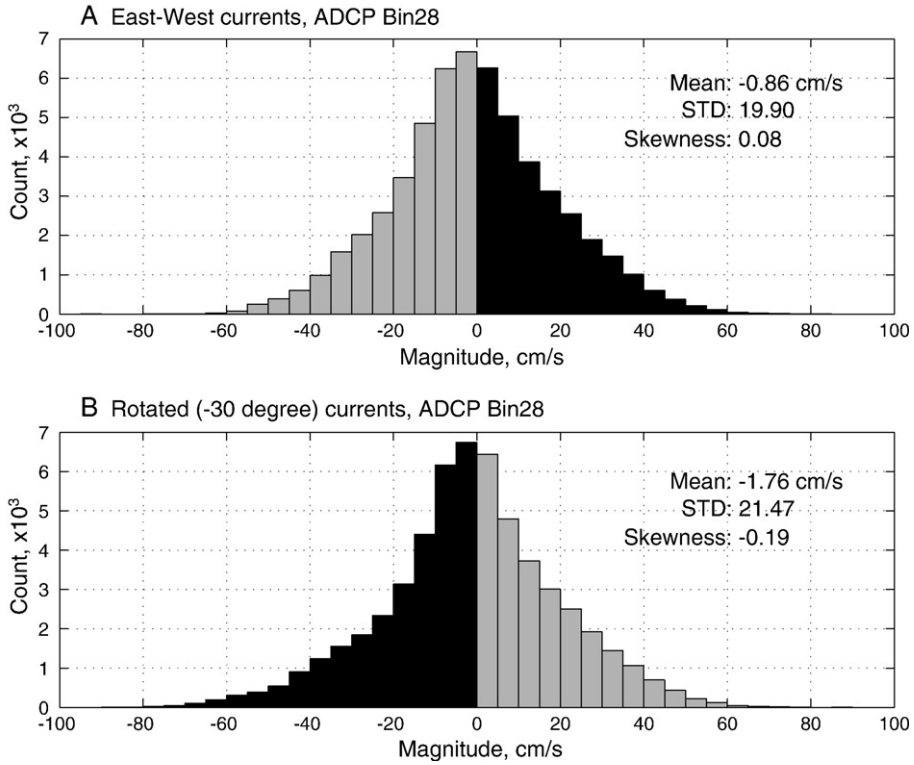

Fig. 7. Histograms of the along-canyon velocity measured 4 MAB. Since the current direction up-canyon is 90°T, but the down-canyon is 300°T, the dark shaded columns represent the 'real' up-canyon (A) and down-canyon (B) currents. Currents of greater than 60 cm/s are dominantly in the down-canyon direction.

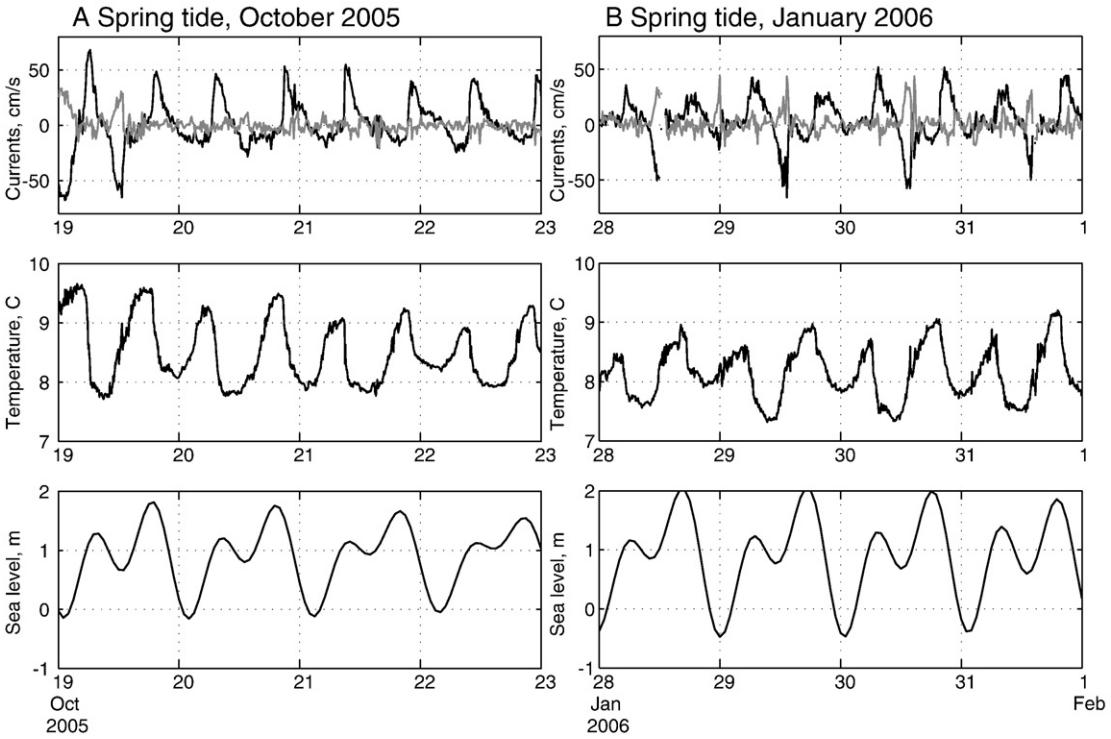

Fig. 8. Time-series plot showing the relationship between currents and temperature measured near the canyon floor during (A) internal bores, and (B) events that have a temporal progression that is the opposite of internal bores. In the two top panels (current velocity) the black lines are along-canyon (up-canyon positive) and the grey lines are cross-canyon currents.

degrees. The second type of flow patterns is almost a reverse image of the first (Fig. 8). The down-canyon current gradually builds up over more than 5 h to the maximum speed of 60–80 cm/s before it rapidly decelerates. The deceleration lasts only ~20 min during which there is no significant change in temperature. Like the internal bores, they occur as packets without apparent relationship with the spring–neap cycle. Both flow patterns are restricted to the near-bed flows, and cannot be found in the upper water column, e.g., 60 MAB. To our knowledge, the second flow pattern has not previously been described. The mechanism of such flow patterns may be related to the localized generation. Kunze et al. (2002) found that, although the energy flux in the canyon is mainly directed up-canyon, in shallower water depths, near the head of the Monterey Canyon, the near-bed energy flux is directed down-canyon, signifying localized generation. Our observation is that the mostly down-canyon strong current is probably due to the same process.

Turbidity currents, though infrequent, are a major driving force for down-canyon sediment transport in submarine canyons. In Monterey Canyon, turbidity currents either have been directly measured or indirectly inferred. Turbidity currents occurred four times in an 11-month monitoring period in 2002–03 with maximum speeds of nearly 200 cm/s (Xu et al., 2004), frequently destroyed or buried bottom-mounted platforms (Paull et al., 2003), and were observed in deep water ranging from 500 to 1400 m. The ADCP mooring described here was located at a shallow site (250 m) where more frequent turbidity currents might occur, assuming most turbidity currents are initiated at the head of the canyon. Surprisingly, the 13-month deployment only recorded one short event that lasted about 10 min (the sampling interval). If it were not for the strong turbidity signals that were generated by the event and oscillated with tides for more than a day before disappearing, the one-data-point event was indistinguishable from "spurious data." The maximum speed of this event was 160 cm/s at ~4 MAB.

3.2. Sizes and shapes of the sandwaves

The sizes (height and wavelength) of the sandwaves are estimated from the wavenumber spectra that are obtained from the lines along the center of the canyon axis (lines 2, 1, and 13). Bathymetric profiles along the three lines from two surveys (5 and 7) that provided the most complete data coverage are used in the spectral analyses.

Table 3
Sizes of the sandwaves calculated from the wavenumber spectra (Fig. 9)

Line no.	Survey no.	X range	Channel gradient	RMS height, (m)	Major wavelengths resolved, (m)
13	5	Overall (30–900)	4°–7°Increasing upslope	1.10	34, 20/18
	7	Overall (30–900)		0.97	28, 19
1	5	Overall (30–900)	2°–6°Increasing upslope	2.34	45, 32, 75
	7	Overall (30–900)		1.63	45, 75
2	5	600–2700	1°–2°	1.22	50/45/40
		2700–3800	1°–4°	1.39	40, 56
		Overall (600–3800)	1°–4° Mostly ≤ 2°	1.29	50, 40
	7	30–1200	See above	1.26	64, 45, 32
		1200–2700		1.35	64, 56/50/45, 32
		2700–4000		1.43	75, 45, 32
		Overall (30–4000)		1.33	45, 64, 32

Sandwaves along lines 13, 1, and 2 (from shallow to deep water, in the middle of the canyon axis) are used in the calculations. The bathymetry has been smoothed using high-pass filter so small wavenumber (wavelength longer than 100 m) sandwaves are not included. Line 2 was divided into two or three sections whose wavenumber spectra were computed separately.

For line 2, the longest, wavenumber spectra are computed over the whole length as well as separately for 2 or 3 sections arbitrarily divided according to the curvature of the canyon (Table 3). The root mean square (RMS) heights of the sandwaves are obtained using $\eta = \sqrt{8m_0}$, where m_0 is the zeroth moment of the wavenumber spectra. The wavelength of the sandwaves, λ, which are the reciprocal of the wavenumber, are directly estimated from the spectra (Fig. 9). In most cases, there is more than one significant peak in the spectra; thus all significant wavenumbers, and wavelengths, are rank-ordered with the first one being the most prominent (Table 3, Fig. 9).

All multibeam maps that have complete coverage of the surveyed area show that the sandwaves at the deeper end have longer apparent wavelengths than their counterparts in the shallow water (Fig. 1). This pattern is clearly consistent with the spectral results (Table 3 and Fig. 9). In both surveys (5 and 7), the wavelengths increased with water depth, from 20–30 m in the area of Line 13, to 30–40 m in the area of Line 1, then to 40–60 m in the area of Line 2. There are differences between the two surveys, for instance along Line 2 the wavelengths during Survey 5 are mostly 40–50 m, compared to the more than 60 m during Survey 7. The down-canyon increase of wavelength seems inversely related to the slope of the canyon floor. The slope along Line 13 is generally greater than 4° while the slope of Line 2 is generally less than 2°. The slope of Line 1 (0–800) is between 2 and 4°.

The height of the sandwaves also varies with water depth (between the lines) but not monotonically as in the case of the wavelength. Instead, sandwaves with the greatest heights are found in Line 1. Here the heights are almost twice as high as in the shallower Line 13, and about 50% greater than in the deeper Line 2 (Table 3). The temporal variation is also the greatest here (Fig. 9). The wave heights during Survey 5, 2.34 m, is almost 40% greater than the Survey 7 wave height, 1.63 m. The explanation in Smith et al. (2007) for the wavelength should also apply here to the wave height—the increased wave height in the Line 1 section were the result of a constricted, therefore narrower channel, where flow speed is responsively higher. Moreover, it is likely the spatial change, not the absolute "narrowness", of the canyon axis channel that affects the size (height and wavelength) of the sandwaves. Stretches of canyon floor in deeper water along Line 2 are even narrower (Fig. 2, Table 3), but the height of the sandwaves there are much smaller than that of the Line 1. The slope of the canyon floor could also be a factor, but it is not a simple linear relationship. Other factors, including the along-canyon flow, must have also played important roles in shaping the sandwaves.

The sizes of the observed sandwaves fit the definition of large dunes that are classified to have wave heights of 0.75–5 m and wavelengths of 10–100 m (Ashley, 1990). The height/length ratios of these sandwaves (Table 3) also appear to be in the vicinity of Flemming, $\eta_{mean} = 0.0677 \cdot \lambda^{0.8098}$, but substantially less than predicted by the maximum global trend, $\eta_{max} = 0.16 \cdot \lambda^{0.84}$. It is also noteworthy that except for the head of the canyon, all sandwaves are crescent shaped with the two tips pointing down-canyon. One such sandwave normally spans the whole canyon width laterally. These sandwaves generally fit the descriptions of submarine barchan dunes which are typically formed in unidirectional flows of 20–80 cm/s, and whose two horns point down-current (Wynn et al., 2002b). The concave down-canyon crest lines could have resulted from lower migration speed at the center of the channel (Ernstsen et al., 2005).

3.3. Directions of sandwave migration

The direction of sandwave migration along the canyon axis is quantitatively determined following the method discussed earlier. For each of the seven surveys (Table 1), seven track lines are drawn along the canyon axis at different locations (Fig. 2). The results for these 49 "realizations" are listed in Table 4. The various symbols in

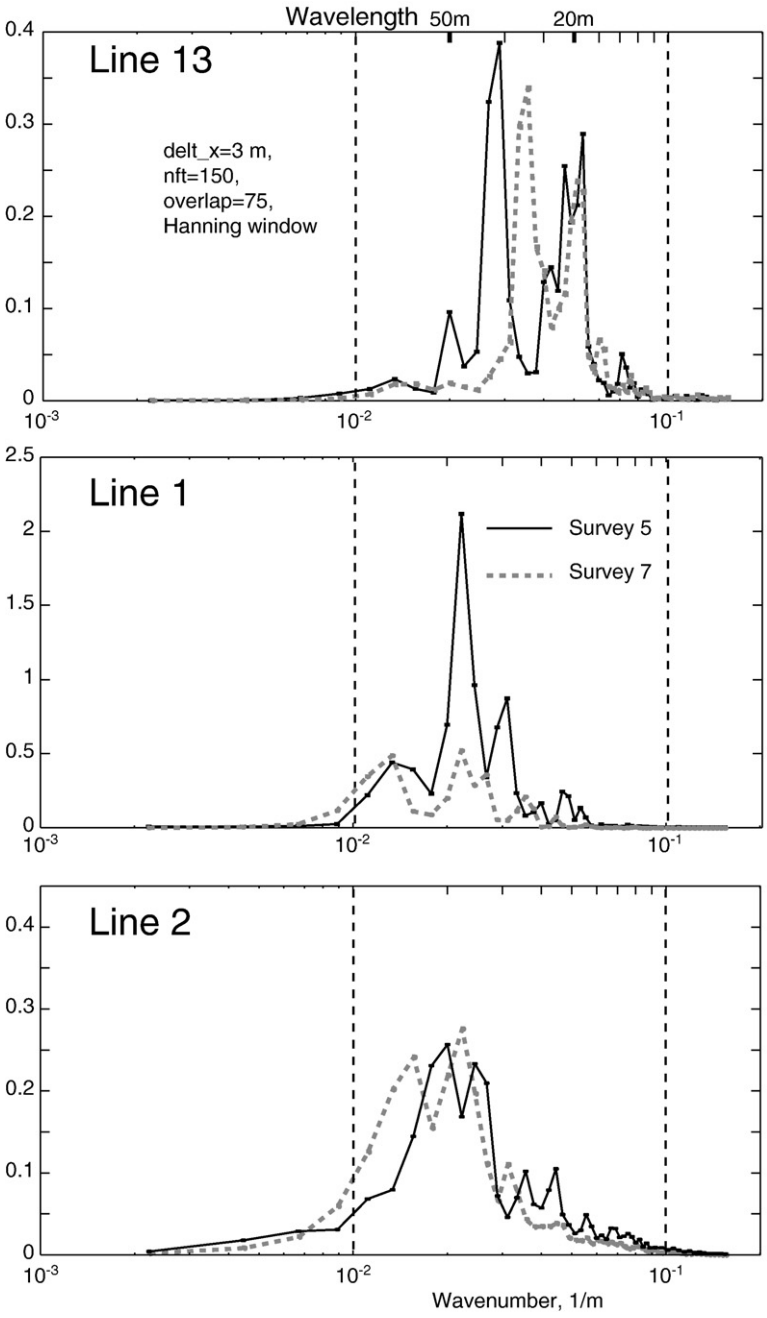

Fig. 9. The "variance preserved" plot of the wavenumber spectra of the sandwave bathymetric profiles from surveys in February 2005 and February 2006 along lines 13 and 1 (both approximately 20–110 m depth), and 2 (110 to 280 m depth), which run along the canyon axis from shallow to deep water. The spectrum was computed using a piece length of 150 m and overlap of 75, with the Hanning window applied. The lengths of the three lines are 900, 1500, and 4000 meters, respectively.

Table 4 represent the degree of the majority of the down- or up-canyon migrations that are calculated from each track line during each survey, two of which are plotted in Fig. 10. The Line1/Survey 5 represents the cases where down-canyon migration is overwhelming (more than 75%). The second case in Fig. 10 represents the other end member in which there are only slightly more down-canyon (51–60%) than up-canyon migration directions.

Table 4 provides a glimpse of the spatial and temporal variation of the sandwave migration within the canyon

Table 4
Direction of sandwave migration estimated by the scheme depicted in Fig. 3

Survey no.	Line 13	Line 14	Line 12	Line 1	Line 3	Line 4	Line 2
1	D	D	D	D/u	D	D	D/u
2	D	D/U	D	D/u	D/u	D/	D/u
3	D	D	D	D/U	D/U	D/u	U/D
4	D/U	D/U	D	D/u	D/U	D/u	
5	D	D/u	D	D	D/u	D	D/u
6	D/u	D/U	D/U	D/u	D/u	D/u	D/U
7	D/u	D	D	D	D	D	D/u

The down-and up-canyon migrations are represented by the letter 'D' and 'U,' respectively. D=overwhelmingly down-canyon (>70%), D/u=down-canyon dominant (61–70%), D/U=slightly more down-canyon (51–60%), U/D=slightly more up-canyon (<50%).

axis. (1) Overall, down-canyon migration is dominant. Except for two cases (one without data) all 7 lines during all seven surveys show that the majority of the sandwaves migrate down-canyon. (2) The sandwave migration is more down-canyon dominant along all track lines in some surveys. For instance, in Surveys 1 and 7, five out of seven track lines have more than 70% of sandwaves migrating down-canyon; and all seven track lines have more than 60% of sandwaves showing down-canyon migration. These two surveys were in different seasons and 4 years apart, but they were both conducted in a similar tidal phase (4 or 5 days after neap tide). Whether this carries any temporal significance is unclear because the near-bed tidal current is not correlated with the surface tidal phase. (3) Although the overall migration is down-canyon, it is more overwhelmingly so along some track lines than along others, regardless of the time of the survey. For example, except for Survey 6, along Line 12 the sandwaves are overwhelmingly down-canyon. In contrast, in Lines 13 and 14, which are parallel to Line 12 in the same stretch of the canyon axis, the down-canyon migration direction is less dominant.

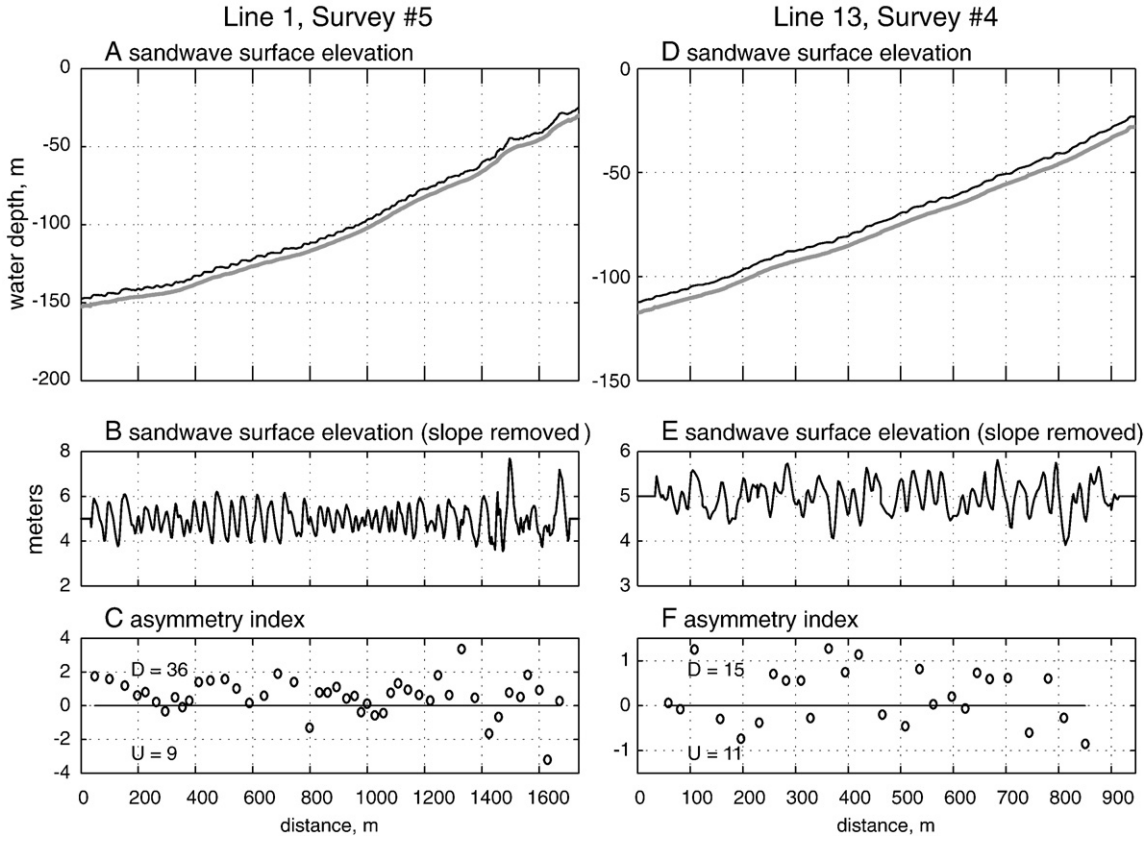

Fig. 10. Asymmetry index of sandwaves calculated from Line 1 in Survey 5, and Line 13 in Survey 4. (A) and (D): Profiles of sandwaves along the two lines. The grey thicker line represents the base slope of the canyon floor. Note the different aspect ratios of the individual sandwaves. (B) and (E) The sandwave surface after the canyon slope has been removed. (C) and (F) The calculated asymmetry index values are positive if sandwaves are migrating down-canyon and negative if up-canyon. The horizontal resolution of the surveys is 3 m. Sandwaves with wavelength less than 2 pixels (6 m) are omitted from this calculation.

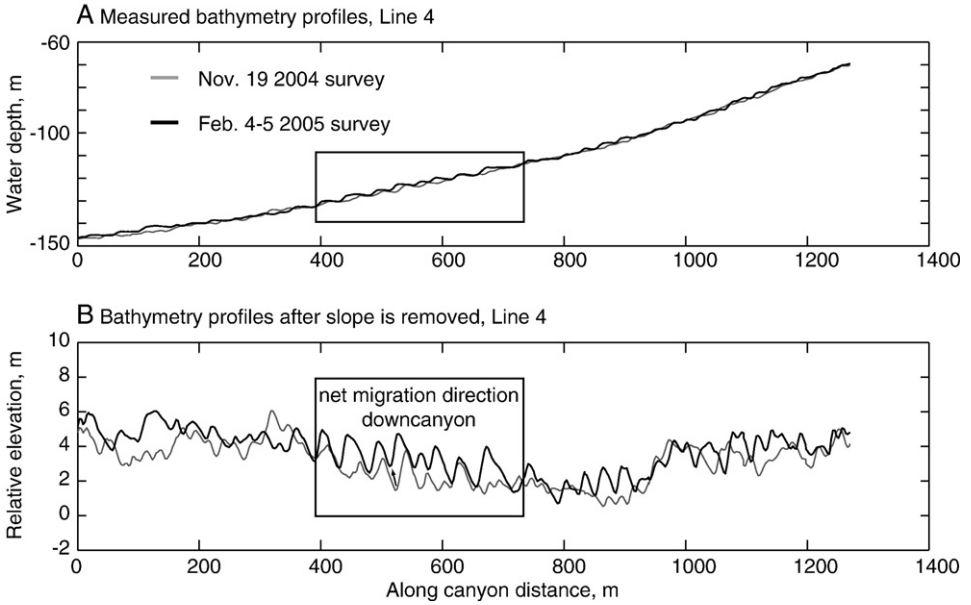

Fig. 11. An example of estimating sandwave migration rate. (A) Measured bathymetric profiles along line 4 during two surveys that were 3 months apart. Vertical exaggeration is 4:1. (B) The same profiles after a common slope is removed. The slope is the smoothed profile of the first survey minus 5 m. The migration rate is measured from the sandwaves within the box. The arrow connects the corresponding sandwaves from both surveys.

3.4. Speeds of sandwave migration

Sequential multibeam images may be used to estimate the direction and magnitude of sandwave migration (Ernstsen et al., 2005; Smith et al., 2007). The accuracy of these estimates depends on the overall quality of the images, the time interval between the surveys, and the regularity of the sandwaves. Sandwaves in two consecutive images may be difficult to correlate due to either the poor quality and/or irregularity of the sandwave field examined, or the potential "aliasing" caused by the long sampling interval between the two surveys. In the 7 multibeam surveys of the Monterey Canyon, the quality of the images varies from one survey to another, but data from sections of the sandwave fields along the canyon axis are consistently good across 2 or 3 consecutive surveys. Since the shortest time span between the surveys was 3 months, we are not sure how "aliasing" has affected the estimate. Smith et al. (2005) seemed to have ruled out variations within one tidal period by comparing two

Table 5
Estimates of sandwave migration distance from visual comparisons of sequential multibeam survey bathymetric profiles

	Line no.	Surveys 3/4	Surveys 4/5
Area L	1	No overlap images	A total of 11 sandwaves can be correlated. The down-canyon migration distances are: 14, 25, 20, 17, 9, 12, 10, 22, 19, 24, and 19 m.
	3	No overlap images	Down-canyon migration: 24, 34, 22, 25, 25 m.
	4	No overlap images	A total of 6 sandwaves can be correlated: 12, 10, 9, 13, 10, and 15 m.
Area S	12	Most of sandwaves that can be correlated are 180° out of phase. Between $X=100$ and 300 m, sandwaves can be said to have migrated up-canyon for 5 m, or down-canyon for 12 to 15 m.	Sandwaves are 180° out of phase. Shifting the profile from Survey 5 either down-or up-canyon by 12 to 15 m similarly aligns the same number of sandwaves.
	13	In the area described in Smith et al. (2007), a train of 4–5 sandwaves migrated 6 m up-canyon	No correlations between the 2 surveys can be positively identified.
	14	Similar to Line 13, sandwaves moved 3 to 5 m up-canyon	By shifting the bathymetric profile from Survey 5 up-canyon for 11 m the sandwaves from both surveys are best in alignment. Thus the migration is about 11 m, down-canyon.

The time intervals between the 3 surveys (Nos. 3, 4, and 5) are roughly 3 months.

surveys conducted 24 h apart, but there is no existing data that would prove or disprove the dependence of sandwave migration on the spring–neap cycle. Noting these uncertainties, we proceed with this test of our method on this unprecedented sequence of high-quality bathymetric images of the canyon floor.

An example of such estimate is shown in Fig. 11. Bathymetric profiles extracted along the canyon axis from two multibeam surveys that were 3 months apart were plotted together. If the two profiles are visually similar, the distances that the sandwaves migrated during the 3-month interval can be determined within the limit of the 3-m horizontal resolution of the multibeam images, with the measuring tools in Adobe Illustrator. The number of estimates that could be made is limited by the number of consecutive surveys with the minimum 3-month interval, the continuous coverage of the targeted areas, and features that can be identified between surveys (Table 5). In Area L where sandwaves are larger, the migration distances amount to 10s of meters. In Area S where smaller sandwaves prevail, the migration distances are in general less than 10 m. The ratio of these measured distances to time (3 months) should be considered the net migration rate of the sandwaves because it is uncertain whether the sandwaves always migrate in one direction.

4. Discussion

4.1. Sandwave generation in submarine canyons

Subaqueous sandwaves have been the subject of numerous studies (for example, Rubin and McCulloch, 1980; Allen, 1982; Flemming, 2000). Although the majority of these studies are oriented to fluvial, estuarine, and other shallow marine environments, most of the hydrodynamic and morphodynamic principles obtained can be used in studying the generation and migration of sandwaves in deep-water environment such as submarine canyons (Wynn et al., 2002a; Smith et al., 2007).

Most sandwave studies treat such bedforms (ripples, sandwaves, dunes) as cyclic depositional/erosional features formed during primarily bedload transport processes. For the sandwaves in the Monterey Canyon, however, another mechanism is being investigated in which the sandwaves are only the surface representations of a down-canyon creep of the whole sand body in the axis of the canyon, which is similar to the topographical forms on the surface of a slowly advancing glacier. Limited by the data available, the discussion in this paper will focus on how the observed sandwaves might have been formed by hydrodynamic forcing and sedimentological and morphological properties of the canyon axis.

Sandwave morphology is controlled by flow velocity, grain size, and water depth or flow depth (Rubin and McCulloch, 1980; Flemming, 2000). Sediment samples taken at different sites along the canyon axis, in different times of different years, have shown that the grain size varies very little with water depth (Mitts, 2003). Both surface grab (McLaren, 2000) and vibracore (Mitts, 2003; Paull et al., 2005) samples taken in the canyon axis indicate that the mean grain size falls into the range of fine sands (0.125–0.25 mm), which is almost indistinguishable from local beach sands in both size and mineralogy (Paull et al., 2005). Using the median value of 0.19 mm as a representative grain size, an empirical relation (Flemming, 2000) produces the maximum possible size of sandwaves as approximately 4 m in height, η, and 60 m in wavelength, λ. Sandwaves in Monterey Canyon have wavelengths similar to the estimate (λ=60 m) (Table 3), but heights are only half of the estimate (η=4 m).

In shallow bays or tidal channels, water depth and flow depth are essentially the same. In submarine canyons the depth of the bottom flows could be very different from flows within and above the canyon in both magnitude and direction due to bottom intensification (Petruncio et al., 1998; Key, 1999; Kunze et al., 2002; Xu et al., 2002). This is evident in Monterey Canyon where the measured velocity at 4 MAB is often greater than that at 60 MAB (Figs. 5 and 6) In these occurrences the bottom flow depth that is relevant to forming bedforms in the canyon axis should be less than 60 m. Applying the "rule of thumb" Yalin (1964) formula, η is equal to 1/6 flow depth h, the heights of the sandwaves should have ranged from 10 m (for h=60 m) to 0.7 m (for h=4 m). This range overestimates the observed η, and is probably caused by the combination of overestimating the flow depth, h, and a flawed empirical constant, 1/6.

Rubin and McCulloch (1980) found that a much smaller empirical constant, 1/10–1/50, should be used in the Yalin (1964) formula in the case of San Francisco Bay sand dunes and therefore modified the Yalin formula such that it also becomes a function of the flow velocity: $\eta/h = 1/6\ (\tau-\tau_c)/\tau$, where τ is the bed shear stress, and τ_c is the critical shear stress for the sand grain. This modified relation shows that when the bottom flow is just above the critical sand mobilization value, the Yalin empirical constant can be much smaller than 1/6. The Yalin constant only approaches its maximum value of 1/6 when the bottom flow becomes very strong, $\tau >> \tau_c$.

For sand beds with mean grain size of 0.19 mm, the critical shear stress is found to be approximately 1.5 dyne/cm^2 (Soulsby, 1997). The bed shear stress can be estimated with a simple quadratic equation, $\tau = \rho C_D U_c^2$, where ρ(=1.026 g/cm^2) is the seawater density; C_D is

the drag coefficient; and U_c is the current speed at 1 m above the canyon floor. The ADCP measurement does not reach 1 MAB, which is too close to the bed, but an empirical formula (Soulsby, 1990) allows the calculation of U_c from a known velocity at heights above 1 MAB: $U_c=(1/h)^{1/7}U_h$, where h is the elevation, in meters, from which the current velocity, U_h, is known and is equivalent to the flow depth. For instance, $U_c=0.72U_{10}$, $U_c=0.62U_{30}$.

Applying a nominal value of the friction coefficient $C_D=2\times10^{-3}$ (Huntley et al., 1994; Green and McCave, 1995; Williams, 1995), and using the top range of current speed ($U_h=50$ and 80 cm/s) demonstrated in Figs. 5 and 6, the current-induced bottom shear stress can be estimated (Table 6). Despite several assumptions such as single grain size and a nominal friction coefficient, the similarity of some estimated sandwave heights to the observed (Table 3) indicates that the tidal currents within the Monterey Canyon are capable of generating the sandwaves observed. In comparison, a 200 cm/s and 30 m thick turbidity current (Xu et al., 2004) would have produced sandwaves as high as 4.8 m by this formula. Sandwaves of this size have not been seen anywhere in the surveyed area, and it is unclear whether this is because the model breaks down for high-speed turbidity currents or the sandwave field have been changed by tidal currents that it no longer reflect the nature of the sandwaves immediately after turbidity current events.

4.2. Sand transport associated with sandwave migrations

When two raster files of the DEM from the same area are subtracted the volume of sediment gain/loss during the time interval between the two DEMs can be estimated (e.g., Smith et al., 2007). If the sediment gains or losses are mainly due to sandwave migration and the time interval between the two DEMs is short enough there should be an alternate gain–loss pattern that resembles the shapes of the sandwave field. Raster subtraction of the two DEMs from 2002 and 2005 shows no patterns that resemble sandwaves (Fig. 2-A in Smith et al., 2007). In contrast, subtractions of DEMs that are approximately 6 months apart reveal a sediment gain–loss pattern that does mimic the sandwave morphology in many areas of the canyon floor (Fig. 12). This infers that sediment transport on the floor of the Monterey Submarine Canyon is at least partially due to sandwave migration.

Table 6
Estimated bed shear stress for the given flow depths (10, 30, and 60 m respectively) and flow speed at the top of the flow (50 and 80 cm/s respectively)

	Bed shear stress, τ, dyne/(cm^2)		Sandwave height, η, (m)	
Flow depth, h, (m)	$U_h=50$	$U_h=80$	$U_h=50$	$U_h=80$
10	2.66	6.81	0.73	1.30
30	1.97	5.05	1.19	3.51
60	1.61	4.12	0.68	6.36

The height of the sandwaves that are generated by such flows is calculated using $\eta/h=1/6\ (\tau-\tau_c)/\tau$. The assumed constants are: $C_D=2\times10^{-3}$, $\tau_c=1.5$ dyne/cm^2.

Large spatial and temporal variations exist in the volumes of sediment gained or lost along the canyon axis in the sandwave field. These estimated volumes are deemed statistically significant because they exceed the error calculated for the vertical resolution of the instrument (Fig. 12). If there is no external input of sediment and the sediment transport is solely due to sandwave migration, the sediment gains and losses calculated from raster subtractions should cancel each other and the net change of sediment volume should be nearly zero. Except for one case (Fig. 12-C), the net change of sediment volume is significantly greater than the calculated error independent of the time interval (2–12 months) between two consecutive DEM surveys.

Our data sets were not collected frequently enough to reveal any temporal pattern. The three surveys (Fig. 12-A, B, F) with similar data coverage and similar time intervals (6 to 7 months) show both gains and losses of sediment. Raster subtractions of DEMs with longer time intervals, either the 12 months in Fig. 12-E or the sum of Fig. 12-A and B, appear to indicate net sediment loss, a result that agrees with a 29-month subtraction of the same area (Smith et al., 2007). When the study area is limited to the head of the canyon (Fig. 12-C, D) the calculation results in a net gain of sediment, which is not unexpected because the total sediment input of 0.25–0.5 millions cubic meters (Best and Griggs, 1991; Paull et al., 2003) from littoral drift and the Salinas River all initially enter the head of the canyon. This volume of sediment is eventually transported and redistributed down-canyon along the axis, and, in geological time-scales, deposited in the deep ocean to create the fan-valley system (Normark and Piper, 1991). Other than sandwave migration, intermittent pulses of "canyon head flushing" (Okey, 1997) have been proposed to move large volumes (not yet quantified) of sediment down-canyon. This flushing is probably also the source of the turbidity currents observed in deep water (Xu et al., 2004).

4.3. Dynamic controls of sandwave migration

Sandwave migration is a complex phenomenon that varies with respect to both time and space. The

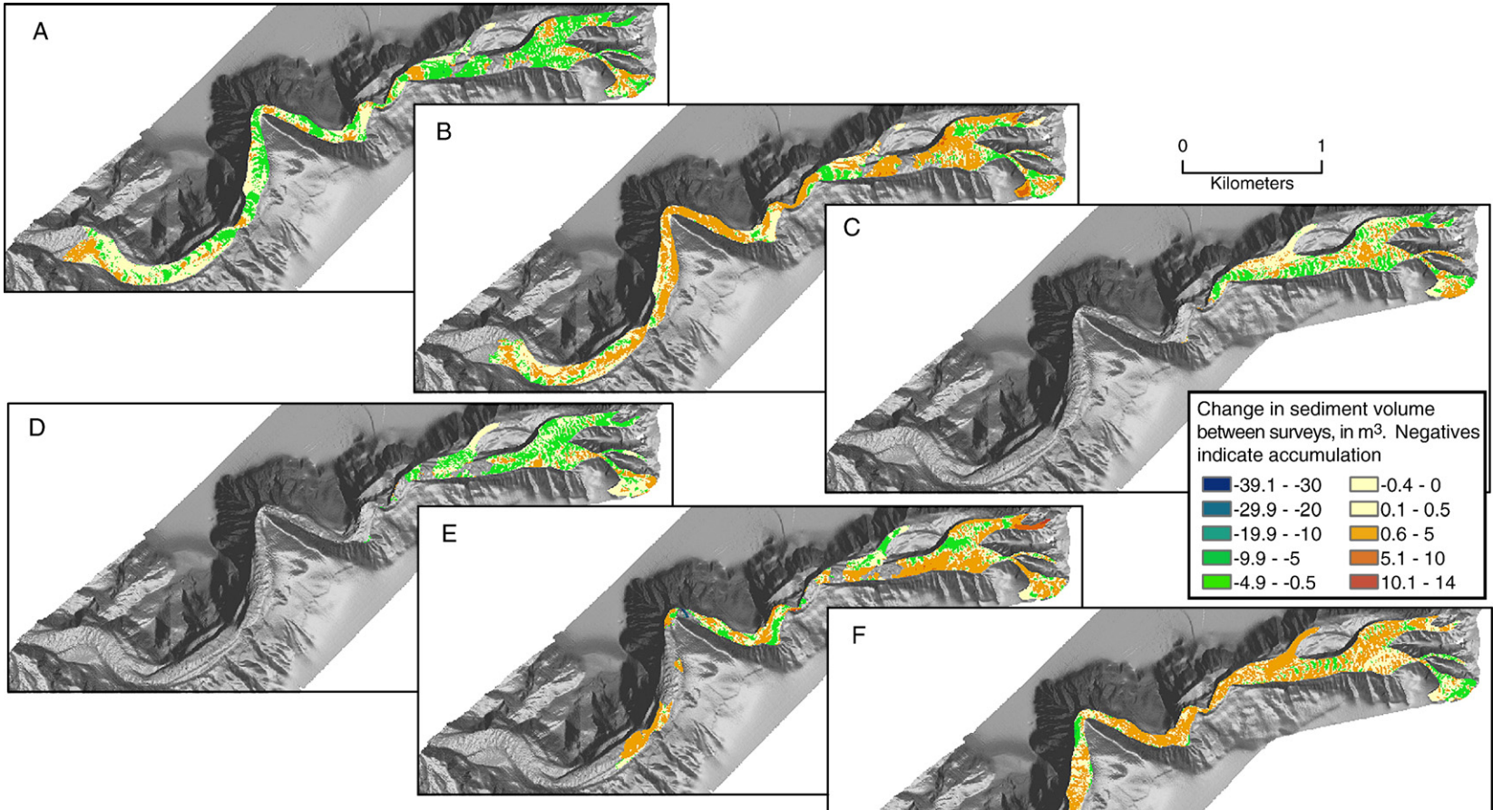

	Interval	Loss	Gain	Net	Total Area	Error
	Days	m^3 x1000	m^3 x1000	m^3 x1000	m^2 x1000	m^3 x1000
A (9/05 - 2/06)	167	180	396	-216	715	143
B (2/05 - 9/05)	217	613	138	475	689	138
C (11/04 - 2/05)	76	127	151	-24	366	73
D (9/04 - 11/04)	63	55	163	-108	315	63
E (9/03 - 9/04)	370	502	151	351	456	91
F (3/03 - 9/03)	170	448	95	353	688	138

Fig. 12. Sediment transport (gain/loss) represented by the raster subtraction of DEMs from different surveys. The colored area is the canyon axis that is bounded between the lowest terraces on both sides of the canyon floor where overlap multibeam data exist. The volumes of gain/loss have been rounded to the nearest 1000 m^3. Given the resolutions of 0.2 m in vertical and 3.0 m in horizontal dimensions, the error bars are estimated by multiplying the vertical resolution (0.2) by the total area considered in each raster subtraction.

mechanisms that create the sandwaves also determine the migration (direction and speed) of the sandwaves. Unless the driving flows are both temporally steady and spatially homogeneous the migration of the sandwaves, just like the sandwave morphology, are expected to be both time and space dependent. Long-term migration is primarily in the direction of residual current (Nemeth et al., 2002; Besio et al., 2004), but tidal oscillations and fortnightly cycles also change the sandwave migration in coastal and estuarine environments (Berne et al., 1993; Besio et al., 2004; Ernstsen et al., 2005).

The multibeam data presented in this paper provided seven "snap shots" of the sandwaves, though some surveys took more than one day (and, therefore, more than one tidal cycle) to complete. Nevertheless they represent a baseline for both the temporal and spatial variations of migration direction of the sandwaves (Table 4). The overall down-canyon migration pattern appears to be independent of the timing, or tidal phase, during which the multibeam surveys were conducted (Table 1). This insensitivity appears to have resulted from the lack of correlation between surface tide and near-bed currents in the axis of the canyon (Figs. 5 and 6) because the observed currents were mainly baroclinic (Fig. 8). The mooring site is not exactly in the sandwave field; therefore, the correlation between the observed currents and the sandwave migration may not be strong. Figs. 5, 6, and 8 do show that, while pulses of strong (50–80 cm/s) baroclinic current with semi-diurnal frequency occur intermittently in both up-and down-canyon directions, the time averages (a proxy of residual currents) during these periods are mostly down-canyon. A short (5 days) mooring deployment by MBARI in 2003 at 125 m water depth also showed pulses of internal tidal currents of ~40 cm/s, but these pulses exclusively pointed up-canyon. It is unknown whether a much longer data time-series at this shallower site would have given a different mean (or residual) current.

In addition to tidal flows, down-canyon turbidity currents affect sandwave migration. No turbidity currents were observed during this study, but previous observations in deeper water (Xu et al., 2004) and frequent damage and burial of instrument platforms (Paull et al., 2003) indicate that turbidity currents occur in the Monterey Canyon. Although uniformly directed down-canyon, turbidity currents can cause sandwaves to migrate up-or down-canyon depending on the internal Froude Number $F_i = U/\sqrt{g'\mathrm{d}}$, where U is the depth-averaged speed, d is the thickness of turbidity currents, $g' = \mathrm{g}(\rho_2 - \rho_1)/\rho_1$ is the "effective gravity", and ρ_1 and ρ_2 are respectively the density of the ambient water and the enhanced density of the turbidity currents. Supercritical turbidity currents, ($F_i > 1$), create antidunes that migrate in the direction opposite to the currents; and subcritical turbidity currents ($F_i < 1$) make dunes (sandwaves) that migrate in the direction of the flows. Using the characteristic thickness of 30 m (see previous discussions) and sediment concentration of 5–10 kg/m^3 (Rosenberger and Xu, 2006) of the observed turbidity currents in the Monterey Canyon, the minimum speed required to produce supercritical conditions is 1.5–1.8 m/s. Such depth-averaged speeds probably occurred since the maximum observed speed was nearly 2.0 m/s, possibly during the surge (Wynn et al., 2002a). The ensuing turbidity currents after the surge are subcritical and would have caused down-canyon migration of the sandwaves. However, as Wynn et al. (2002a,c) pointed out, the influence of turbidity currents on sandwave migration is likely much more complicated than what the simple internal Froude Number can possibly describe. At present time there are just insufficient data and knowledge to fully determine the relationship between episodic turbidity currents and observed sandwaves.

4.4. Issues in determining sandwave migration from bathymetry

Advances in survey technologies provide high-quality, high-resolution, 3-dimensional bathymetric images that can reveal bed features at centimeter scales. However, it is still difficult to quantify the sandwave migration (direction and speed) from such data collected in an environment of oscillating flows, especially when there is a large time gap (months) between the sequential multibeam images, as is the case in the present data set. The first challenge is to quantify the asymmetry of the sandwaves, which holds the most direct relationship to the migration direction. Unlike the sandwaves in river channels or in bi-directional tidal inlets where sandwave asymmetry can be clearly identified (Ernstsen et al., 2005), the sandwaves in the axis of the Monterey Canyon are much more complex in size, shape, and orientation. One source of complexity is the canyon itself, whose width, slope, and surrounding bathymetry vary substantially from the head down. Opposing sandwave asymmetries co-exist in a small area, and neither the positive or negative asymmetry may be statistically dominant. Moreover, several different sizes of sandwaves co-exist, and they are not always superimposed on each other. The asymmetry of one size of sandwaves may be the opposite of the other. A filter technique may be applied to focus on the asymmetry of sandwaves of one particular size, but the resulting asymmetry can be different from that of the original data.

A more difficult task is to assess the migration speed of the sandwaves from these images. Raster subtraction of two DEMs is a popular and straightforward way and has

been successfully used (Ernstsen et al., 2005; Knaapen, 2005; Wienberg and Hebbeln, 2005; Ernstsen et al., 2006), where the time interval is short (hours to days) between the two consecutive DEM surveys. When the time intervals are as long as in the current paper (3 months to a year) it becomes very difficult to identify the most prominent individual sandwaves in the two DEMs, much less between groups of sandwaves. In such cases, image processing software (2-dimensional Fourier transform, for instance) does not work. Even when correspondences can be made between sandwaves in the two DEMs, it is still uncertain whether "aliasing" is present. These critical time-interval issues need to be explored further when using sequential DEMs. Although the morphodynamic timescale is much larger than the characteristic hydrodynamic timescale (Besio et al., 2004), more frequent observations of the sandwaves, probably with surveys other than the multibeam bathymetry, such as rotating scan sonar, are needed.

5. Conclusion

A sequence of high-resolution multibeam bathymetry surveys allowed us to closely examine the migrations of the sandwaves in the Monterey Submarine Canyon. Sandwaves were found on the floor along the canyon axis in the whole surveyed section, from 20 to 250 m water depth. The height and wavelength of the sandwaves ranged approximately 1–2 m and 30–60 m, respectively. While maximum sandwave heights were found in a section of intermediate water depth (100–150 m), there is a subtle trend of growing wavelength with increasing water depth. This trend coincides with a down-canyon decrease of canyon slope.

The sandwave migration directions (up-vs down-canyon) were determined by a method based on the asymmetries of the observed sandwaves. Despite spatial variations along the canyon, the migration direction is dominantly down-canyon in all seven surveys that took place during different tidal phases in different seasons. From a limited number of survey pairs where sandwaves could be well correlated, it was determined that sandwaves in some sections migrated 10s of meters down-canyon during a 3-month interval.

Tidal and internal tidal currents dominated the canyon flows recorded at 250 m water depth, which was at the deeper end of the multibeam surveys. Intermittent packets of strong currents (maximum observed speed of 50–80 cm/s) were often bottom intensified (strongest near the bed). Because these strong pulses are not correlated with surface tides, they are likely related to internal tides. Assuming the same flow amplitude within the sandwave field along the axis of the canyon, a simple empirical model showed that such flows could have generated sandwaves of the observed sizes.

The down-canyon migration in general coincided with the down-canyon residual currents—a relationship that has been observed in fluvial channels and tidal inlets. This dataset, however, is not adequate to allow formulating a relationship between the sandwave "snap shots" and the dynamic flows observed. Experiments designed to collect concurrent flows and sandwave properties could help address these issues.

Acknowledgement

We thank Pat Iampietro and the staff and students of the Seafloor Mapping Lab of the CSUMB for their efforts in collecting and processing the multibeam data during and following the cruises on R/V *MacGinitie* and R/V *Ven-Tresca*, The manuscript benefited from frequent discussions with Dave Rubin. Jessie Lacy, Dave Rubin, Serge Berne and Russell Wynn provided insightful reviews that ultimately strengthen the paper. We acknowledge the various sources of funding that supported the collection and processing of the different multibeam data sets: NOAA Monterey Bay National Marine Sanctuary, NOAA Cooperative Institute for Coastal and Estuarine Environmental Technology (CICEET), NOAA Center for Integrative Coastal Observation, Research, and Education (CICORE), and USGS Coastal and Marine Geology Program.

References

Allen, J.R.L., 1968. Current Ripples: Their Relation to Patterns of Water and Sediment Motion. North-Holland, Amsterdam.

Allen, J.R.L., 1980. Sandwaves: a model of origin and internal structure. Sediment. Geol. 26, 281–328.

Allen, J.R.L., 1982. Sedimentary structures: their character and physical basis, vol. 1. Developments in sedimentology series, vol. 30. Elsevier, New York. 593 pp.

Ashley, G.M., 1990. Classification of large-scale subaqueous bedforms: a new look at an old problem. J. Sediment. Petrol. 60, 160–172.

Barnard, P.L., Hanes, D.M., Kvitek, R.G., Iampietro, P.J., 2006, Sand waves at the mouth of San Francisco Bay, California: U.S. Geological Survey Scientific Investigations Map 2944, 5 pls., [URL http://pubs.usgs.gov/sim/2006/2944/].

Bartholdy, J., Flemming, B.W., Bartholoma, A., Ernstsen, V.B., 2005. Flow and grain size control of depth-independent simple subaqueous dunes. J. Geophys. Res. 110, F04S16. doi:10.1029/2004/JF000183.

Berne, S., Castaing, P., Le Drezen, E., Lericolais, G., 1993. Morphology, internal structure, and reversal of asymmetry of large subtidal dunes in the entrance to Gironde estuary (France). J. Sediment. Petrol. 63 (5), 780–793.

Besio, G., Blondeaux, P., Brocchini, M., Vittori, G., 2004. On the modeling of sand wave migration. J. Geophys. Res. 109, C04018. doi:10.1029/2002JC001622.

Best, T.C., Griggs, G.B., 1991. A sediment budget for the Santa Cruz littoral cell, California. In: Osborne, R.H. (Ed.), From Shoreline to Abyss: Contributions in Marine Geology in Honor of Francis Parker Shepard. Society for Sedimentary Geology Special Publication, vol. 46, pp. 35–50.

Coleman, J.M., 1969. Brahmaputra River: channel process and sedimentation. Sediment. Geol. 3, 129–239.

Dalrymple, R.W., 1984. Morphology and internal structure of sandwaves in the Bay of Fundy. Sedimentology 31, 365–382.

Drake, T.G., Calantoni, J., 2001. Discrete particle model for sheet flow sediment transport in the nearshore. J. Geophys. Res. 106, 19859–19868.

Eittreim, S.L., Xu, J.P., Noble, M.A., Edwards, B.D., 2002. Towards a sediment budget for the Santa Cruz shelf. Mar. Geol. 181, 235–248.

Ernstsen, V.B., Noormets, R., Winter, C., Hebbeln, D., Bartholoma, A., Flemming, B.W., Bartholdy, J., 2005. Development of subaqueos barchanoid-shaped dunes due to lateral grain size variability in a tidal inlet channel of Danish Wadden Sea. J. Geophys. Res. 110, F04S08. doi:10.1029/2004JF000180.

Ernstsen, V.B., Noormets, R., Winter, C., Hebbeln, D., Bartholoma, A., Flemming, B.W., Bartholdy, J., 2006. Quantification of dune dynamics during a tidal cycle in an inlet channel of the Danish Wadden Sea. Geo Mar. Lett. 26, 151–163.

Fildani, A., Normark, W.R., 2004. Late Quaternary evolution of channeland lobe complexes of Monterey fan. Mar. Geol. 206, 199–223.

Flemming, B.W., 2000. The role of grain size, water depth and flow velocity as scaling factors controlling the size of subaqueous dunes. In: Trentesaux, A., Garlan, T. (Eds.), Marine Sandwave Dynamics, Proceedings of and Internaltional Workshop held in Lille, France, 23–24 March 2000. University of Lille 1, Lille, pp. 55–60.

Francken, F., Wartel, S., Parker, R., Taverniers, E., 2004. Factors influencing subaqueous dunes in the Scheldt Estuary. Geo Mar. Lett. 24, 14–24.

Garfield, N., Rago, T.A., Scnebele, K.J., Collins, C.A., 1994. Evidence of a turbidity current in Monterey Submarine Canyon associated with the 1989 Loma Prieta earthquake. Cont. Shelf Res. 14, 673–686.

Green, M.O., McCave, I.N., 1995. Seabed drag coefficient under tidal currents in the eastern Irish Sea. J. Geophys. Res. 100 (C8), 16057–16069.

Greene, H.G., Ward, S.N., 2003. Mass movement features along the central California margin and their modeled consequences for tsunami generation. In: Locat, J., Mienert, J. (Eds.), Submarine Mass Movements and their Consequences, Advances in Natural and Technological Hazards Research. Kluwer Academic Publishers, Boston, pp. 343–356.

Hoekstra, P., Bell, P., van Santen, P., Roode, N., Levoy, F., Whitehouse, R., 2004. Bedform migration and bedload transport on an intertidal shoal. Cont. Shelf Res. 24, 1249–1269.

Huntley, D.A., Nicholls, R.J., Liu, C., Dyer, K.R., 1994. Measurements of semi-diurnal drag coefficient over sand waves. Cont. Shelf Res. 14, 105–132.

Kalkwijk, J.P.T., Booij, R., 1986. Adaptation of secondary flow in nearly-horizontal flow. J. Hydraul. Res. 24, 19–37.

Katoh, K., Kume, H., Kuroki, K., Hasegawa, J., 1998. The development of sand waves and the maintenance of navigation channels in the Bisanseto Sea. In: Edge, B.L. (Ed.), Coastal Engineering 1998: Conference Proceedings. Am. Soc. Civ. Eng., Reston, VA, pp. 3490–3502.

Key, S., 1999. Internal tidal bores in the Monterey Canyon. Thesis, Naval Postgraduate School. 91pp.

Knaapen, M.A., 2005. Sandwave migration predictor based on shape information. J. Geophys. Res. 110, F04S11. doi:10.1029/2004JF000195.

Kunze, E., Rosenfeld, L.K., Carter, G.S., Gregg, M.C., 2002. Internal waves in Monterey Submarine Canyon. J. Phys. Oceanogr. 32, 1890–1913.

Leopold, L.G., Wolman, M.G., 1960. River meanders. Geol. Soc. Amer. Bull. 71, 769–793.

McLaren, P., 2000. A sediment trend analysis (STA) and an acoustic bottom classification (ABC) in Eastern Monterey Bay, Moss Landing: implication to dredge disposal operations. Final report for Moss Landing Harbor District. 106pp.

Mitts, P.J. 2003. Deposition and provenance of modern coarse sediment in Monterey Submarine Canyon. Thesis, San Jose State University. 186pp.

Morelissen, R., Hulscher, S.J.M.H., Knaapen, M.A.F., Nemeth, A.A., Bijker, R., 2003. Mathematical modeling of sand wave migration and the interaction with pipelines. Coast. Eng. 48, 197–209.

Nemeth, A.A., Hulscher, S.J.M.H., de Vriend, H.J., 2002. Modelling sand wave migration in shallow shelf seas. Cont. Shelf Res. 22, 2795–2806.

Normark, W.R., Carlson, P.R., 2003. Giant submarine canyons: is size any clue to their importance in the rock record? In: Chan, M.A., Archer, A.W. (Eds.), Extreme Depositional Environments: Mega End Members in Geologic Time: Boulder, Colorado. Geol. Soc. Am., Spec. Pap., vol. 370, pp. 170–190.

Normark, W.R., Piper, D.J.W., 1991. Initiation processes and flow evolution of turbidity currents: implications for the depositional record. In: Osborne, R.H. (Ed.), From Shoreline to Abyss. SEPM Spec. Publ., vol. 46. SEPM, Tulsa, OK, pp. 207–230.

Okey, T.A., 1997. Sediment flushing observations, earthquake slumping, and benthic community changes in Monterey Canyon head. Cont. Shelf Res. 17, 877–897.

Paull, C.K., Ussler III, W., Greene, H.G., Keaten, R., Mitts, P., Barry, J., 2003. Caught in the act: the 20 December 2001 gravity flow event in Monterey Canyon. Geo Mar. Lett. 22, 227–232.

Paull, C.K., Ussler III, W., Keaten, R., Mitts, P., Greene, H.G., 2005. Trail of sand in upper Monterey Canyon. Geol. Soc. Amer. Bull. 117, 1134–1145.

Petruncio, E.T., Rosenfeld, L.K., Paduan, J.D., 1998. Observations of the internal tide in Monterey Canyon. J. Phys. Oceanogr. 28, 1873–1903.

Rosenberger, K., Xu, J.P., 2006. Estimating the volume of downcanyon sediment transport by turbidity currents. EOS Trans. AGU 87 (36). Ocean Sci. Meet. Suppl., OS45A-06.

Rubin, D.M., McCulloch, D.S., 1980. Single and superimposed bedforms: a synthesis of San Francisco Bay and flume observations. Sediment. Geol. 26, 207–231.

Smith, D.P., Ruiz, G., Kvitek, R., Iampietro, P.J., 2005. Semi-annual patterns of erosion and deposition in upper Monterey Canyon from serial multibeam bathymetry. Geol. Soc. Amer. Bull. 117, 1123–1133.

Smith, D.P., Kvitek, R., Iampietro, P.J., Wong, K., 2007. Twenty-nine months of geomorphic change in upper Monterey Canyon (2002–2005). Mar. Geol. 236, 79–94.

Soulsby, R.L., 1990. Tidal-current boundary layers. In: LeMehaute, B., Hanes, D.M. (Eds.), The sea. Ocean Engineering Science, vol. 9B. Wiley, New York.

Soulsby, R.L., 1997. Dynamics of marine sands. Thomas Telford, London.

Van den Berg, J.H., 1987. Bedform migration and bed load transport in some rivers and tidal environments. Sedimentology 34, 681–698.

Wienberg, C., Hebbeln, D., 2005. Impact of dumped sediments on subaqueous dunes, outer Weser Estuary, German Bight, southeastern North Sea. Geo Mar. Lett. 25, 43–53.

Williams, J.J., 1995. Drag and sediment dispersion over sand waves. Estuar., Coast. Shelf Sci. 41, 659–687.

Wynn, R.B., Piper, D.J.W., Gee, M.J.R., 2002a. Generation and migration of coarse-grained sediment waves in turbidity current channels and channel-lobe transition zones. Mar. Geol. 192, 59–78.

Wynn, R.B., Masson, D.G., Bett, B.J., 2002b. Hydrodynamic significance of variable ripple morphology across deep-water barchan dunes in the Faroe–Shetland Channel. Mar. Geol. 192, 309–319.

Wynn, R.B., Stow, D.A.V., Kenyon, N.H., Masson, D.G., Weaver, P.P.E., 2002c. A new model for deep-water channel-lobe transition zones based on high-resolution seafloor mapping and modern and ancient analogues. Sedimentology 49, 669–695.

Xu, J.P., Noble, M.A., Eittreim, S.L., Rosenfeld, L.K., Schwing, F.B., Pilskaln, C.H., 2002. Distribution and transport of suspended particulate matter in Monterey Canyon, California. Mar. Geol. 181, 215–234.

Xu, J.P., Noble, M.A., Rosenfeld, L.K., 2004. In-situ measurements of velocity structure within turbidity currents. Geophys. Res. Lett. 31, L09311. doi:10.1029/2004GL019718.

Yalin, M.S., 1964. Geometrical properties of sand waves. Proc. Am. Soc. Civ. Eng., J. Hydraul. Div. 90, 105–119.